論文 / 著書情報
Article / Book Information

Title	Seismic Analysis of Wind-Induced Damaged Seismically Isolated Tall Buildings
Authors	X. Qian, D. Sato
Pub. date	2020, 9
Citation	2020 17WCEE Proceedings

17th World Conference on Earthquake Engineering, 17WCEE
Sendai, Japan - September 13th to 18th 2020

Seismic Analysis of Wind-Induced Damaged Seismically Isolated Tall Buildings

X. Qian[(1)], D. Sato[(2)]

[(1)] *Japan, Tokyo Institute of Technology, qian.x.aa@m.titech.ac.jp*
[(2)] *Japan, Tokyo Institute of Technology, sato.d.aa@m.titech.ac.jp*

Abstract

A seismic isolation system is designed to reduce the seismic responses of a building, and it has been applied to more and more tall buildings. However, for those seismically isolated tall buildings in the design for wind, large and long-duration wind loads such as typhoons may cause violent and continuous vibration of the buildings. Because the isolation story is soft, in which the steel dampers (so-called U-shaped steel dampers mounted in the isolation story) behave plastically easily, large residual deformation in the isolation story and fatigue damage in the steel dampers may occur in a typhoon. However, if a great earthquake follows, for those wind-induced damaged seismically isolated tall buildings, larger seismic responses and fatigue damage may occur compared with undamaged buildings. In the previous studies, the residual deformation in the isolation story has been verified based on typhoon observation data, and the fatigue damage in the steel dampers has been calculated by rain-flow counting method and Miner's rule to indicate that the wind-induced damage could not be neglected. However, if there is an initial wind-induced residual deformation in the isolation story, it may influence the seismic responses and fatigue damage in the following earthquakes. Therefore, by carrying out continuous typhoon and seismic simulation, this study investigates the seismic responses and fatigue damage to explore the influences of initial wind-induced residual deformation.

Fig. 1 shows a reduced MDOF model with 11 lumped masses (11 stories). The upper 10 masses (1st ~ 10th story) indicate the upper structure, while the bottom mass (0th story) indicates the isolation story. By continuous typhoon and seismic simulation (Taft 1952 NS), the maximum displacement distribution Dis_{max} (Fig. 2) and maximum acceleration distribution Acc_{max} (Fig. 3) in the seismic simulation were obtained. It was found that the model with initial wind-induced residual deformation of 9cm in the isolation story shows a larger maximum displacement compared with the model without initial residual deformation (Fig. 2). However, the initial residual deformation hardly influenced the maximum acceleration (Fig. 3). Besides, about the fatigue damage (D value) in the steel dampers in the NS direction, the D value of 0.006 was found to occur in the seismic simulation considering the initial residual deformation. However, the D value of 0.004 occurred when there is no initial residual deformation.

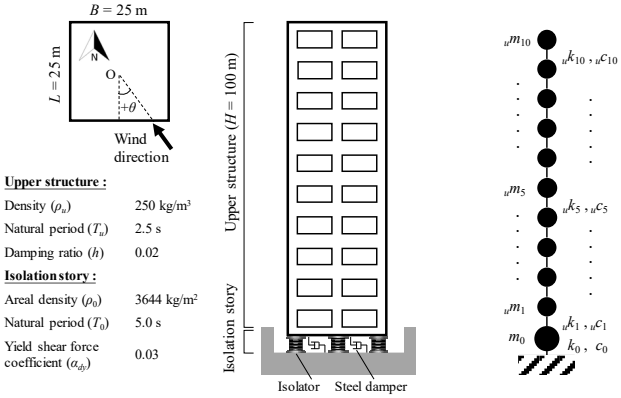

Fig. 1 Structural model

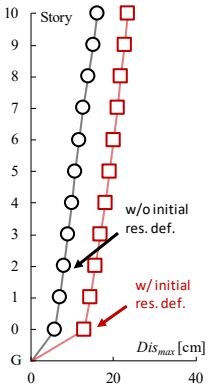

Fig. 2 Max. displacement (NS)

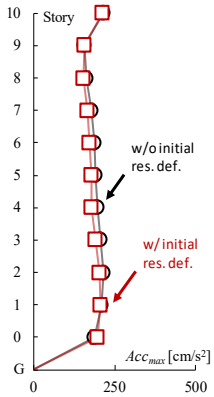

Fig. 3 Max. acceleration (NS)

Keywords: seismically isolated building, wind-induced damage, seismic analysis, residual deformation, fatigue damage

1. Introduction

A seismic isolation system proves to be efficient in reducing the seismic responses of a building, and it has been applied to more and more tall buildings[1] to meet the demands of people. However, for those seismically isolated tall buildings in the design for wind, large and long-duration wind loads such as typhoons may cause violent and continuous vibration of the buildings. Because the isolation story is soft, in which the steel dampers (so-called U-shaped steel dampers mounted in the isolation story) behave plastically easily, large residual deformation[2] in the isolation story and fatigue damage[3] in the steel dampers may occur in a typhoon. However, if a great earthquake follows, for those wind-induced damaged seismically isolated tall buildings, larger seismic responses and fatigue damage may occur compared with undamaged buildings. The previous study[4] shows that the residual deformation in the isolation story has been verified based on typhoon observation data, and the fatigue damage has been calculated to indicate that the wind-induced damage could not be neglected. However, if there is an initial wind-induced residual deformation in the isolation story, it may influence the seismic responses and fatigue damage in the following earthquakes. Therefore, by carrying out continuous typhoon and seismic simulation, this study investigates the seismic responses and fatigue damage to explore the influences of initial wind-induced residual deformation.

In this paper, a reduced MDOF model is described based on a given seismically isolated building. Also, 10 assumed typhoon samples and 4 observed seismic waves (EI Centro 1942, Taft 1952, Hachinohe 1968 and Kobe 1995) are described. The continuous typhoon and seismic simulation were conducted by time history analysis to investigate the seismic responses including the residual deformation and maximum deformation in the isolation story, as well as the maximum displacement and maximum acceleration at the top of the building. The authors tried to explore the influence of initial residual deformation on above simulation results. Besides, the fatigue damage in the steel dampers was calculated by rain-flow counting method and Miner's rule, on which the influence of initial residual deformation was explored as well.

The remaining paper is organized as follows: Section 2 presents the structural model and its structural properties. The outlines of typhoon and seismic simulation are described in Section 3. The simulation results of seismic responses are presented in Section 4. The evaluation of fatigue damage in the steel dampers is also presented in this section. Finally, conclusions and related remarks are presented in Section 5.

2. Structural model

Fig. 1(a) shows the outline of a seismically isolated building. For the upper structure, the height H = 100 m, the breadth B = 25 m, and the Depth L = 25 m. The Density ρ_u = 250 kg/m^3, the natural period T_u = 2.5 s (= 0.025H), and the damping ratio h = 0.02. For the isolation story, the areal density ρ_0 = 3644 kg/m^2, the natural period T_0 = 5.0 s (= 2T_u), and the yield shear force coefficient of the steel dampers α_{dy} = 0.3. About the building orientation, the building breath B is north-south facing, and the northward wind direction is defined as θ = 0°. As shown in Fig.1(b), the MDOF model is reduced to have 11 lumped masses[5] (11 stories) according to the seismically isolated building. The upper 10 masses (1st ~ 10th story) indicate the upper structure, while the bottom mass (0th story) indicates the isolation story. ${}_um_i$, ${}_uc_i$ and ${}_uk_i$ are the mass, damping and stiffness of the i^{th} story of the upper structure, while m_0, c_0 and k_0 are the mass, damping and stiffness of the isolation story, respectively.

According to the above structural parameters, the i^{th} story mass of the upper structure ${}_um_i$ is plotted in Fig. 2(a). Also, as shown in Fig. 2(b), the 1st mode shape of the upper structure is assumed as a straight line, so the i^{th} story stiffness of the upper structure ${}_uk_i$, given by Eq. (1)[6], is plotted in Fig. 2(c).

$$ {}_uk_i = \frac{{}_{us}\omega^2 \cdot {}_um_i \cdot {}_{us}\phi_i + {}_uk_{i+1}\left({}_{us}\phi_{i+1} - {}_{us}\phi_i\right)}{{}_{us}\phi_i - {}_{us}\phi_{i-1}} \tag{1} $$

where ${}_{us}\omega$ and ${}_{us}\phi_i$ are the natural frequency and s^{th} mode eigenvector of the upper structure, respectively. However, ${}_{us}\phi_0$ = 0 and ${}_uk_{11}$ = 0, because the 0th and 11th story are non-existent in the upper structure.

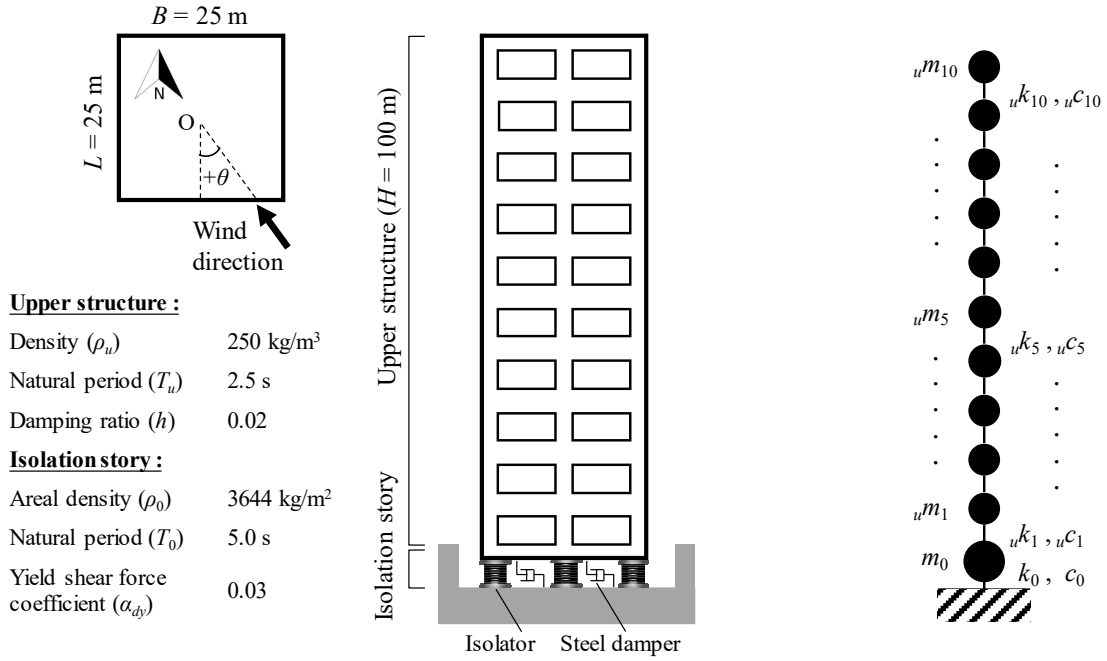

Upper structure :

Density (ρ_u)	250 kg/m^3
Natural period (T_u)	2.5 s
Damping ratio (h)	0.02

Isolation story :

Areal density (ρ_0)	3644 kg/m^2
Natural period (T_0)	5.0 s
Yield shear force coefficient (α_{dy})	0.03

(a) outline of the seismically isolated building (b) the reduced 11-DOF model

Fig. 1 – Structural model

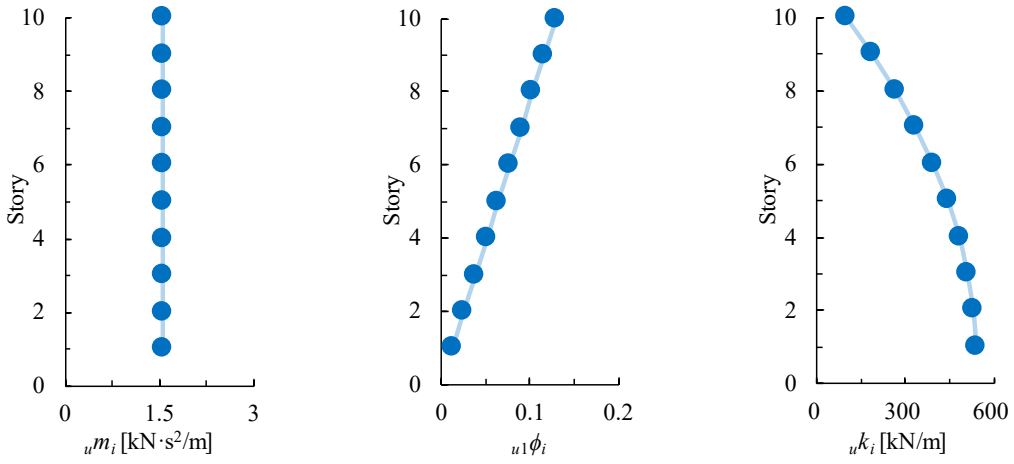

(a) mass (b) 1st mode shape (c) stiffness

Fig. 2 – Structural properties of the upper structure

Fig. 3(a) ~ (c) show the restoring force properties of the steel dampers, isolators and isolation story, respectively. In this study, the performance decrement of the steel dampers (Fig. 3(a)) under long-duration cyclic loading is not considered. The isolators (Fig. 3(b)) are assumed as a kind of elastomeric rubber bearing without lead core. And the restoring force property of the isolation story (Fig. 3(c)) is the combination of the damper property and isolator property.

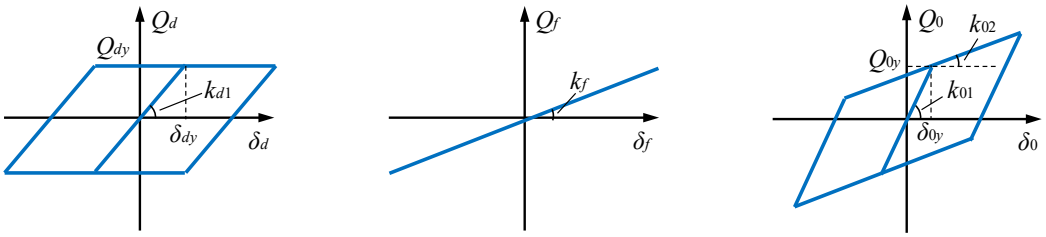

(a) steel dampers (b) isolators (c) isolation story

Fig. 3 – Restoring force properties of the isolation story

According to Fig. 3, the yield load of the steel dampers Q_{dy}, the initial stiffness of the steel dampers k_{d1}, and the stiffness of the isolators k_f can be expressed by Eq. (2) ~ (4).

$$Q_{dy} = (W_u + W_0) \cdot \alpha_{dy} \tag{2}$$

$$k_{d1} = Q_{dy} / \delta_{dy} \tag{3}$$

$$k_f = \frac{4\pi^2 (W_u + W_0)}{T_0^2 \cdot g} \tag{4}$$

where W_u and W_0 are the weight of the upper structure (= 153125 kN) and the weight of the isolation story (= 22319.5 kN), respectively. α_{dy} and δ_{dy} are the yield shear force coefficient (= 0.03) and yield deformation (= 2.80 cm) of the steel dampers, respectively. T_0 is the natural period of the isolation story (= 5.0 s), and g is the acceleration of gravity (= 9.8 N/kg).

According to the above results, the 1st stiffness k_{01}, 2nd stiffness k_{02}, and yield load Q_{0y} of the isolation story can be obtained by Eq. (5) ~ (7).

$$k_{01} = k_{d1} + k_f \tag{5}$$

$$k_{02} = k_f \tag{6}$$

$$Q_{0y} = k_{01} \cdot \delta_{dy} \tag{7}$$

3. Outlines of typhoon and seismic simulation

The continuous typhoon and seismic simulation of the 11-DOF model were carried out by time history analysis. In the typhoon simulation, because of the breadth to depth ratio B/L = 1, the torsion effect of the building under wind force is tiny[7], which can be ignored. In the seismic simulation, there is no torsion effect because of the building with uniform density. Therefore, the torsion effect is not considered in this paper.

3.1 Typhoon simulation

As shown in Fig. 4, 10 assumed typhoon samples with different duration (9 ~ 40 hours) are considered in the typhoon simulation[8]. Fig. 4(a) shows the time history of mean wind speed U_z averaged over each 10 minutes at the height z = 100 m above ground. According to Japanese Recommendations for Loads on Buildings[9], the peak mean wind speed of 50.41 m/s is obtained based on basic wind speed of 36 m/s, 500-year return period and surface roughness III. From Fig. 4(a), it can be seen that Sample 6 (1st peak: 49.54 m/s, 2nd peak: 50.41 m/s), Sample 8 (1st peak: 50.41 m/s, 2nd peak: 48.21 m/s) and Sample 9 (1st peak: 50.41 m/s, 2nd peak: 45.13 m/s) have two peaks, while the other samples have only one peak (peak: 50.41 m/s). Fig. 4(b) shows the time history of wind direction θ over each 10 minutes. From Fig. 4 and 5, each sample shows that the wind direction is fixed at θ = 0° (northward) as the mean wind speed reaches the peak of 50.41 m/s. The maximum wind force, which may lead to a large residual deformation, may occur in the north direction

rather than in the east-west (EW) direction. Therefore, in the typhoon and seismic simulation, the results in the north-south direction (NS) are focused in this paper.

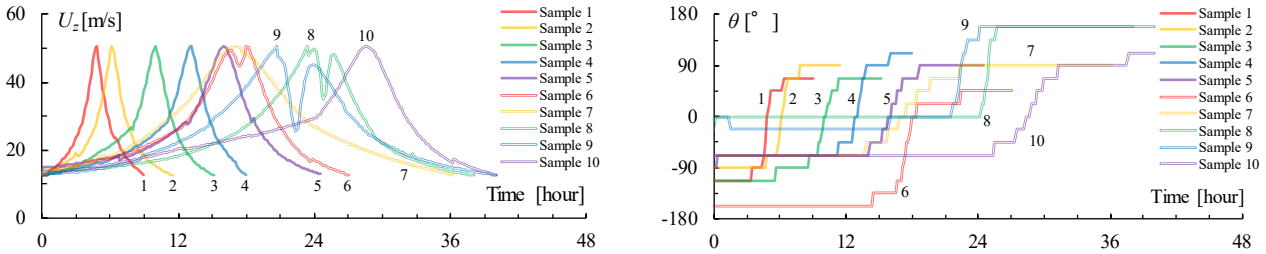

(a) time history of mean wind speed (z = 100 m) (b) time history of wind direction

Fig. 4 – 10 assumed typhoon samples in the typhoon simulation

According to above time history of mean wind speed and wind direction, the i^{th} story wind force of upper structure ${}_uF_i$ can be expressed by Eq. (8)[9].

$$ {}_uF_i = \frac{1}{2}\rho \cdot U_z^2 \cdot {}_uC_i \cdot {}_uA_i \tag{8} $$

where ρ is air density (=1.22 kg/m^3), ${}_uC_i$ is the i^{th} story aerodynamic coefficient of the upper structure obtained from a wind tunnel test[10], and ${}_uA_i$ is the i^{th} story projected area of the upper structure (= 250 m^2).

Fig. 5(a) and (b) show the time history of 10th story wind force ${}_uF_{10}$ (NS) in Sample 1 and 6 at a time interval of 0.05s, respectively. It can be seen that Sample 1 and 6 show the same maximum wind force of over 800kN in the north direction because the wind direction of all typhoon samples is fixed at θ = 0° (northward) as the mean wind speed reaches the peak value. However, in the south direction, the maximum wind force in Sample 6 shows a much larger value than that in Sample 1, because Sample 6 has two peaks in the mean wind speed.

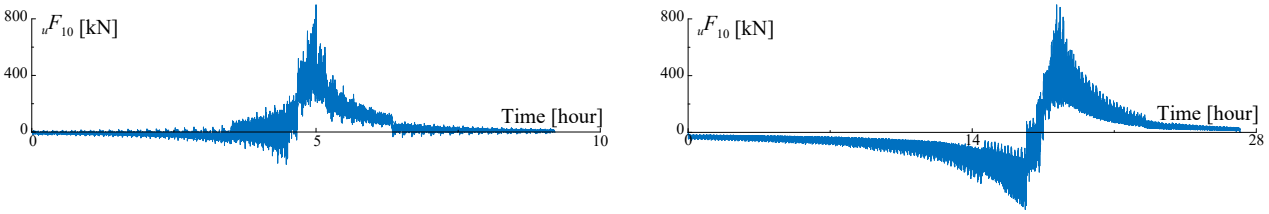

(a) Sample 1 (b) Sample 6

Fig. 5 – Time history of 10th story wind force (NS)

3.2 Seismic simulation

As shown in Table 1, four observed seismic waves in Japan[11] are considered in the seismic simulation, and the ground acceleration (NS) of the four representative seismic waves at a time interval of 0.02s are shown in Fig. 6(a) ~ (d). It can be seen that the Kobe 1995 seismic wave with the longest duration shows a much larger maximum ground acceleration of 820.6cm/s^2 than those in the other three seismic waves. In this study, because of continuous typhoon and seismic simulation, a complete simulation contains one typhoon sample and one seismic wave. Moreover, the typhoon simulation was conducted prior to the seismic simulation.

Table 1 – The four observed seismic waves in Japan

Seismic wave	Direction	Max. acc [cm/s^2]	Durarion [s]	Time interval [s]
El Centro 1940	NS	341.7	54	0.02
Taft 1952	NS	152.7	54	0.02
Hachinohe 1968	NS	229.6	51	0.02
Kobe 1995	NS	820.6	150	0.02

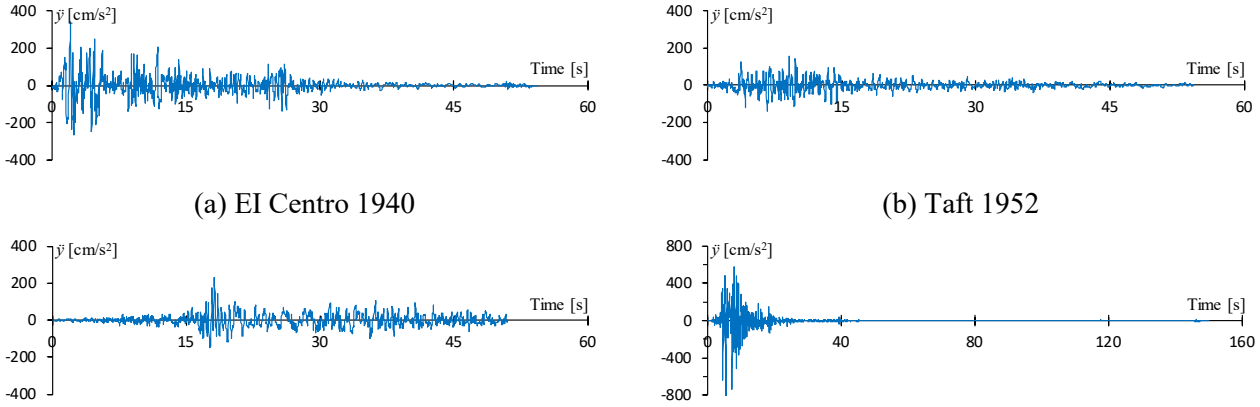

(a) EI Centro 1940 (b) Taft 1952

(c) Hachinohe 1968 (d) Kobe 1995

Fig. 6 – Ground acceleration of the observed seismic waves (NS)

4. Simulation Results

4.1 Residual deformation in the isolation story

Fig. 7(a) shows the simulation result of residual deformation in the isolation story δ_{0r}. The black lines, regarded as initial wind-induced residual deformation, indicate the residual deformation of Sample 1 ~ 10 in the typhoon simulation. It can be seen that the value in Sample 5 reached about 10cm in the north direction, while the value in Sample 8 reached about -7cm in the south direction. As mention in Section 3.1, the maximum wind force occurred in the north direction, which may lead to a large residual deformation in this direction. However, from Fig. 7(a), the residual deformation not always occurred in the north direction. Because of the change in wind direction, the southward wind force may push the model in the opposite direction. According to the typhoon simulation result, it was found that the strong wind led to a large residual deformation in the isolation story. Besides, the plots with different colors in Fig. 7(a) indicate the residual deformation in the following seismic simulation. It can be seen that all the values in seismic simulation are within ±3cm, which are much lower than above initial wind-induced residual deformation. Therefore, the seismic waves can help reduce the residual deformation in the seismic simulation. Moreover, for each seismic wave, the values hardly changed regardless of the initial residual deformation. The residual deformation in the seismic simulation seems to be non-sensitive to the change in initial residual deformation. Fig. 7(b) shows the influence of initial residual deformation in the isolation story. It can be seen that as the initial residual deformation changes from -15cm to +15cm, the residual deformation in the seismic simulation still hardly changed even though the initial residual deformation reached -15cm or +15cm. Therefore, it was found that the initial residual deformation hardly influenced the residual deformation in the seismic simulation.

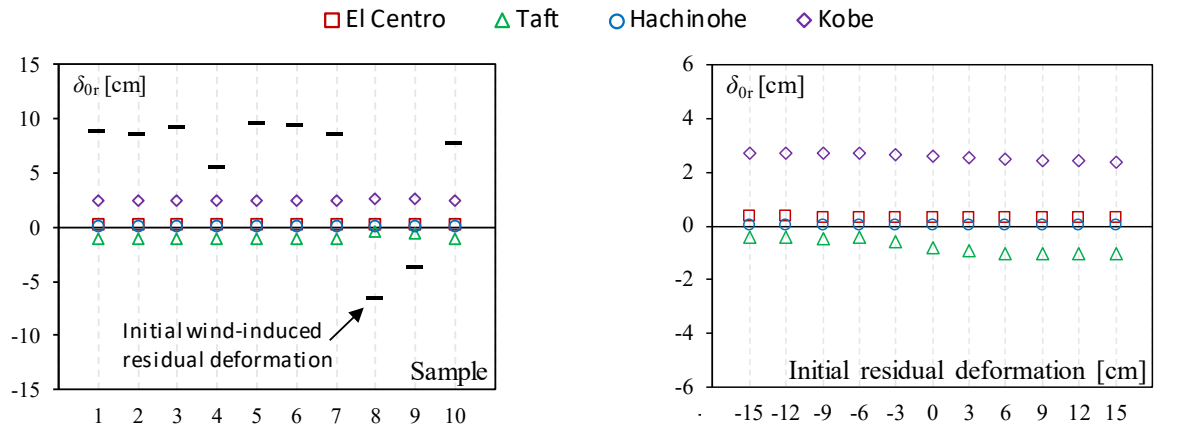

(a) simulation result (b) influence of initial residual deformation

Fig. 7 –Residual deformation in the isolation story (NS)

4.2 Maximum deformation in the isolation story

Fig. 8(a) shows the seismic simulation result of maximum deformation in the isolation story δ_{0max}. The plots with different color still indicate the results of the four seismic waves. It can be seen that the result of EI Centro (red) and Taft (green) shows a lower value after typhoon simulation of Sample 8 and 9. However, the result of Kobe (purple) shows a larger value after typhoon simulation of Sample 8 and 9. From Fig. 7(a), only Sample 8 and 9 show the initial residual deformation occurred in the south direction, which influenced the maximum deformation in the following seismic simulation. Fig. 8(b) shows the influence of initial residual deformation in the isolation story. It can be seen that as the initial residual deformation changes from -15cm to +15cm, for each seismic wave, there is an obvious change in the maximum deformation in the seismic simulation. It is considered that the model with initial residual deformation of 0cm may show a lower value like Taft (green). However, for EI Centro (red), the minimum value was found to occur as the initial residual deformation is -6cm. And for Hachinohe (blue) and Kobe (purple), the minimum value occurred as the initial residual deformation is 9cm. Therefore, certain initial residual deformation in the isolation story can help reduce the maximum deformation in the isolation story in the seismic simulation.

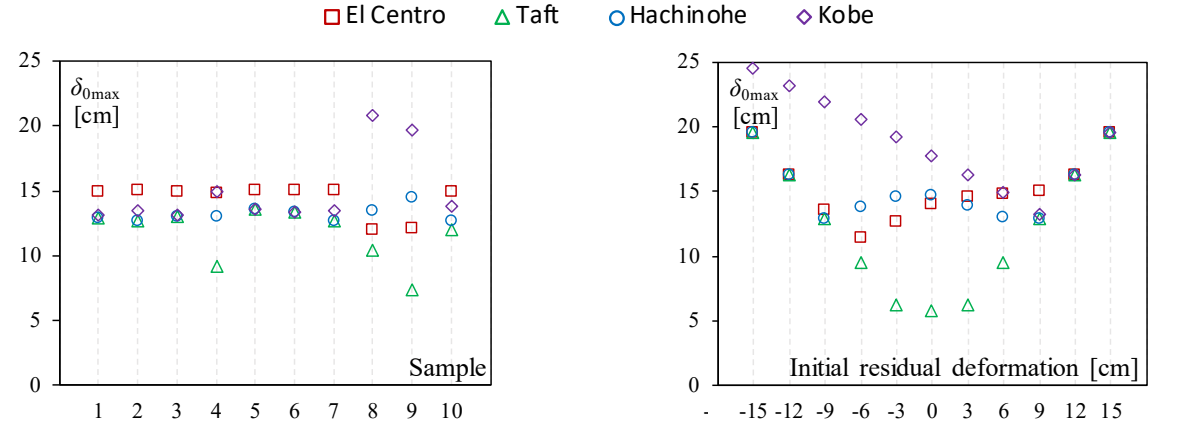

(a) simulation result (b) influence of initial residual deformation

Fig. 8 –Maximum deformation in the isolation story (NS)

4.3 Maximum displacement at the 10th story

Fig. 9(a) shows the seismic simulation result of maximum displacement at the 10th story Dis_{10max}. Similarly, it can be seen that the value of Taft (green) and Hachinohe (blue) shows a lower value after typhoon simulation of Sample 8 and 9, and the value of Kobe (purple) shows a larger value after typhoon simulation of Sample 8 and 9. Therefore, the initial residual deformation influenced the maximum displacement at the 10th story in the seismic simulation. Fig. 9(b) shows the influence of initial residual deformation in the isolation story. Similarly, it can be seen that as the initial residual deformation changes from -15cm to +15cm, for each seismic wave, the values of the 10th story maximum displacement changed in the seismic simulation. It is considered that the model with initial residual deformation of 0cm may show a lower value. However, for EI Centro (red), the minimum value was found to occur as the initial residual deformation is -9cm. For Taft (green), the minimum value occurred as the initial residual deformation is +3cm. For Hachinohe (blue), the minimum value occurred as the initial residual deformation is -3cm. And for Kobe (purple), the minimum value occurred as the initial residual deformation is +6cm. From Fig.9, it was found that the result is similar to that in Section 4.2 Therefore, certain initial residual deformation in the isolation story can also help reduce the 10th story maximum displacement in the seismic simulation.

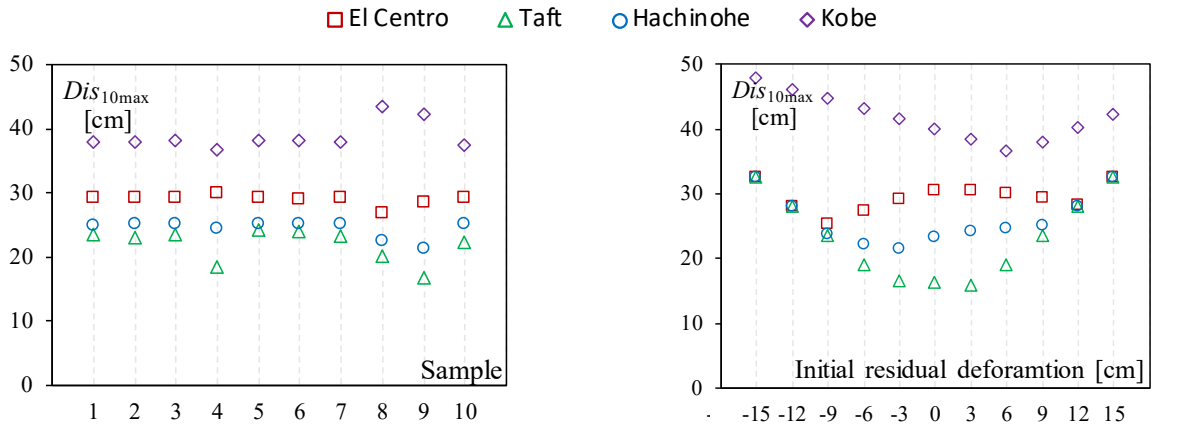

(a) simulation result (b) influence of initial residual deformation

Fig. 9 –Maximum displacement at the 10th story (NS)

4.4 Maximum acceleration at 10th story

Fig. 10(a) shows the seismic simulation result of maximum acceleration at the 10th story Acc_{10max}. From Fig. 10(a), it can be seen that for each seismic wave, the values hardly changed regardless of the initial residual deformation in the isolation story. The 10th story maximum acceleration in the seismic simulation seems to be non-sensitive to the change in initial residual deformation like Section 4.1. Moreover, the values in Kobe (purple) show much larger values than those in the other three seismic waves. Fig. 10(b) shows the influence of initial residual deformation in the isolation story. It can be seen that as the initial residual deformation changes from -15cm to +15cm, the values of the 10th story maximum acceleration slightly changed in the seismic simulation. Even though the initial residual deformation reached -15cm or +15cm, there is still no obvious change in the 10th story maximum acceleration. Unlike the result in Section 4.3, it was found that certain initial residual deformation can not help reduce the 10th story maximum acceleration in the seismic simulation. Therefore, the initial residual deformation in the isolation story hardly influenced the maximum acceleration at the 10th story in the seismic simulation.

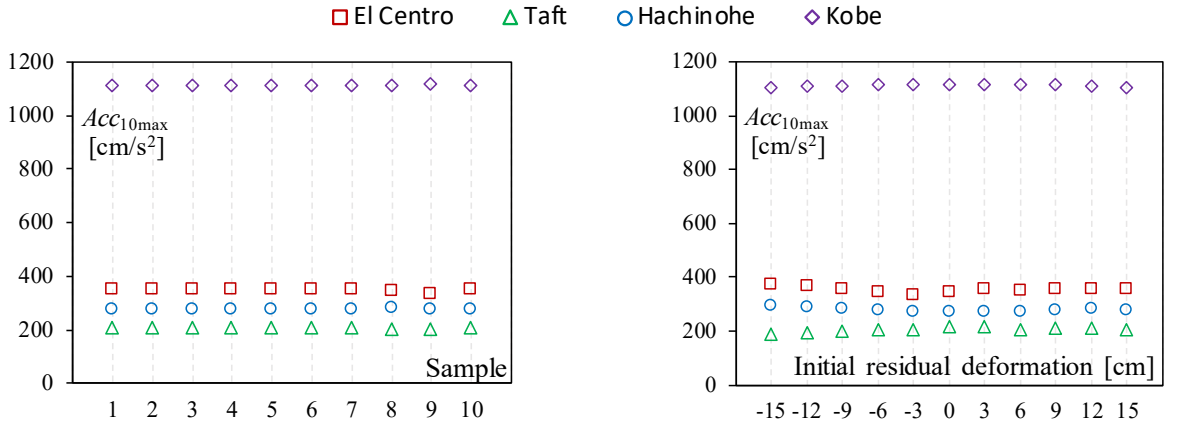

(a) simulation result (b) influence of initial residual deformation

Fig. 10 –Maximum acceleration at the 10th story (NS)

4.5 Fatigue damage in the steel dampers

The fatigue damage in steel dampers (D value) can be expressed as Eq. (9) [12] by using rain-flow counting method and Miner's rule according to the experimental fatigue performance of steel dampers[13].

$$D = \sum D_k = \sum_{k=1}^{np} \frac{N_k}{N_{f(\delta_k)}} \tag{9}$$

where D_k is the fatigue damage degree of double amplitude δ_k, np is the total number of δ_k, N_k is the cycle number of δ_k, and $N_{f(\delta k)}$ is the number of cycles to failure in δ_k.

Fig. 11(a) ~ (d) show the computing result of D value in the typhoon simulation (Sample 1 ~ 10) and seismic simulation (EI Centro, Taft, Hachinohe and Kobe). From Fig. 11(a), it can be seen that the D value of Sample 2 shows the minimum, while the D value of Sample 6 shows the maximum. Although, as shown in Fig. 4(a), the peak mean wind speed of all samples is the same and the duration of Sample 9 and 10 is the longest, the maximum D value occurred in Sample 6 rather than in Sample 9 and 10. Therefore, these D values depend on not only the wind speed and typhoon duration but also the change in wind direction. Regarding the D values in the seismic simulation of EI Centro, it can be seen that all D values are similar to each other. The D values of EI Centro seem to be non-sensitive to the initial wind-induced residual deformation in the isolation story. Also, the D values of EI Centro show a larger value than those in the typhoon simulation of Sample 2 and 3. Although the duration of typhoon is much longer than that of seismic waves, the amplitude of the model in the seismic simulation is much larger due to large seismic force, which may lead to a larger D value. However, both the D values of typhoon and seismic simulation are within 0.05 in the NS direction, and the sum of D values in one typhoon simulation and one seismic simulation is still tiny. So there is no need to worry about the fatigue fracture in the steel dampers after one typhoon and one earthquake. From Fig. 12(b) ~ (d), the D values of Taft show a lower value and the D values of Hachinohe and Kobe show a larger value compared with Fig. 11 (a).

Fig. 12 shows the influence of initial residual deformation in the isolation story. For EI Centro and Taft, the maximum D value occurred as the initial residual deformation is 0cm. For Hachinohe and Kobe, the maximum D value occurred as the initial residual deformation is +3cm. From Fig. 12, it can be seen that, for each seismic wave, the D values were slightly influenced by the initial residual deformation. However, because the D values themselves in the seismic simulation are tiny, the influence of initial residual deformation could be neglected.

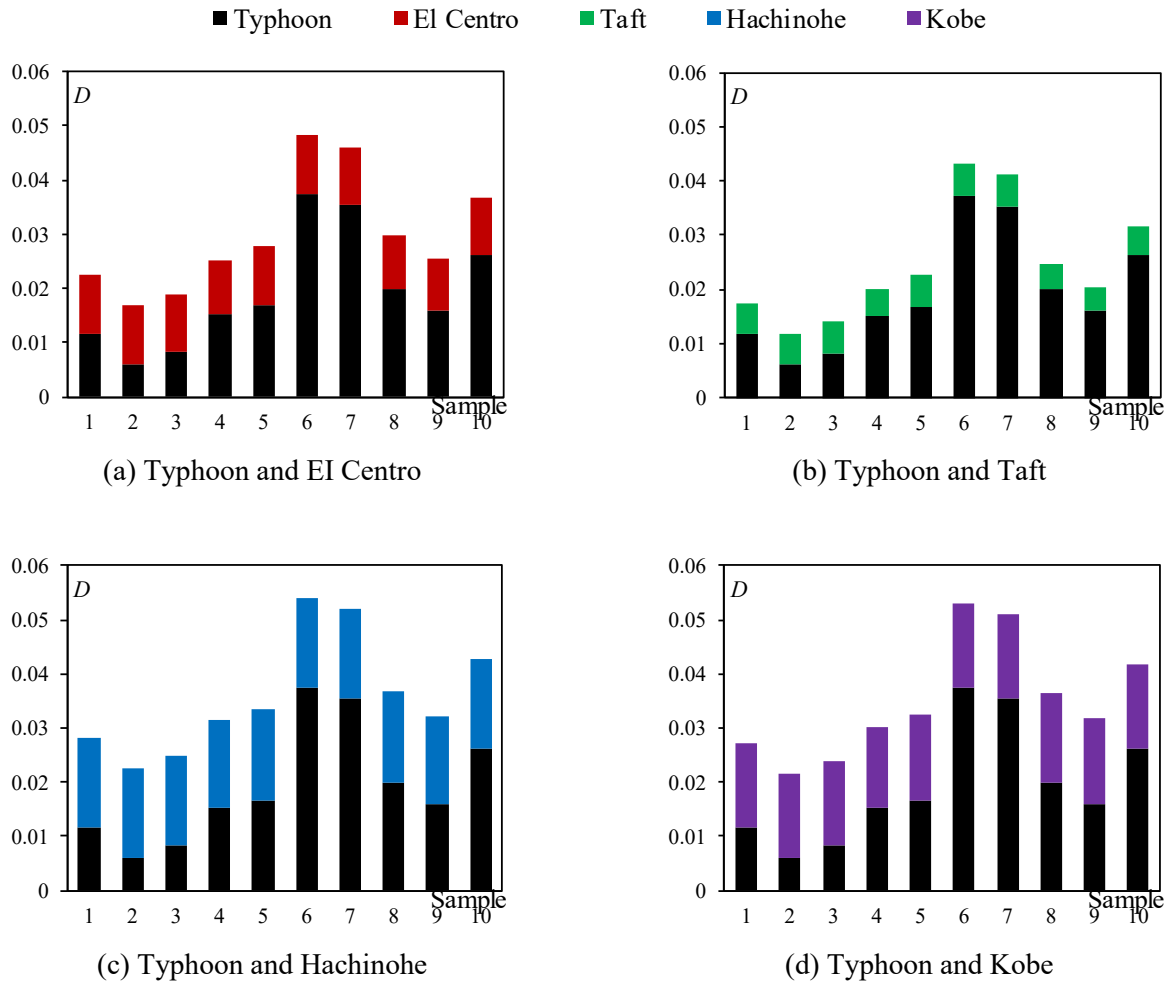

(a) Typhoon and EI Centro

(b) Typhoon and Taft

(c) Typhoon and Hachinohe

(d) Typhoon and Kobe

Fig. 11 –Computing result of *D* value in typhoon and seismic simulation (NS)

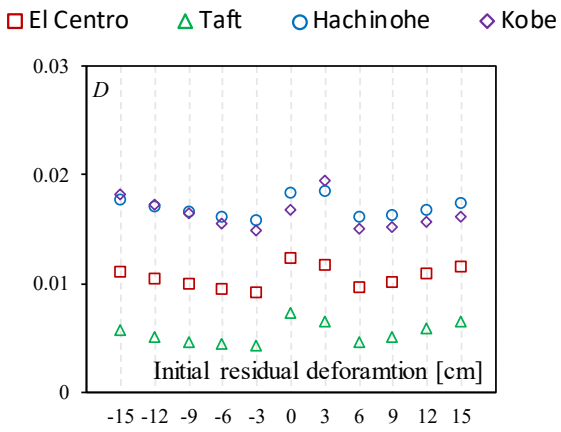

Fig. 12 –Influence of initial residual deformation on *D* value (NS)

5. Conclusions

By conducting continuous typhoon and seismic simulation, this paper investigated the seismic responses of seismically isolated buildings considering initial wind-induced residual deformation in the isolation story. From the seismic simulation results, the maximum displacement at the 10th story and maximum deformation in the isolation story were influenced by the initial residual deformation. And certain initial residual deformation can help reduce these seismic responses. However, the residual deformation and the 10th story maximum acceleration in the seismic simulation were hardly influenced by the initial residual deformation. Moreover, regarding the fatigue damage in the steel dampers, the *D* values were slightly influenced by the initial residual deformation. However, because the *D* values themselves in the seismic simulation are tiny, the influence of initial residual deformation could be neglected.

In this paper, only one type of seismically isolated building is considered. However, it may come to a different conclusion if there is a change in the natural period of the isolation story or the yield shear force coefficient of the steel dampers. Furthermore, a prediction method for seismic responses of seismically isolated buildings considering large initial residual deformation is needed to be proposed.

6. Acknowledgements

This work was supported by JST Program on Open Innovation Platform with Enterprises (JPMJOP1723), Research Institute and Academia. Also, the authors would like to thank Nishijima Laboratory in Kyoto University for providing precious typhoon simulation data, Izumisohken Engineering Co., Ltd. for providing precious wind tunnel test data, and Nikken Sekkei Ltd for valuable advice in this research work.

7. References

[1] The Japan Society of Seismic Isolation (2019): Chronological data on buildings with seismic isolation & vibration control, 2018FY. *MENSHIN*, No. 105, 21-26. (Japanese)

[2] Qian X, Sato D (2020): Evaluation of residual deformation in seismic isolation layer based on typhoon simulation, *Journal of Structural Engineering*, Vol. 66B. (Japanese)

[3] Qian X, Sato D, Mabashi S (2019): Effects of building aspect ratio on fatigue damage of steel dampers installed in base-isolated high-rise buildings. *The 15th International Conference on Wind Engineering*, *Proceedings of the 15th International Conference on Wind Engineering*, 563-564.

[4] Murakami T, Sato D, Tamura T, Fugo Y, Yoshie K, Kasai K, Sato T, Kitamura H (2016): Actual behavior of seismic isolated high-rise building based on observation records at strong wind. *Journal of Structural Engineering*, Vol. 62B, 329-337. (Japanese)

[5] Katagiri J, Ohkuma T, Yasui H, Marukawa H, Tsurumi T (2011): Study of accuracy for reduced model of high-rise buildings with base isolation systems. *AIJ Journal of Technology and Design*, No. 36, 461-466. (Japanese)

[6] Sato D, Kasai K, Tamura T (2009): Influence of frequency sensitivity of viscoelastic damper on wind-induced response. *Journal of Structural and Construction Engineering*, Vol. 74, No. 635, 75-82. (Japanese)

[7] Mabashi S, Sato D (2019): Wind response analysis using a three-dimensional analysis model of a high-rise isolation building, *Journal of Structural Engineering*, Vol. 65B, 1-8. (Japanese)

[8] Danguri N, Nishijima K (2018): Method for selecting hazard-consistent most-likely typhoon based on probabilistic typhoon model, *DPRI Annual Meeting*, B19. (Japanese)

[9] Architectural Institute of Japan (2015): Recommendation for loads on buildings, 321-434. (Japanese)

[10] Marukawa H, Ohkuma T, Kitamura H, Yoshie K, Tsurumi T, Sato D (2010): Energy input of local wind forces for high-rise building based on wind tunnel test: Part. 2 Local wind force characteristics of rectangular high-rise buildings. *Summaries of technical papers of annual meeting*, Vol. B-1, 193-194. (Japanese)

[11] Building Performance Standardization Association. (Japanese)

[12] Murakami T, Sato D, Tamura T, Fugo Y, Ikegami M, Yoshie K, Kasai K, Kitamura H (2015): Fatigue damage evaluation of the steel material damper of high-rise seismic isolated building based on observation data. *Journal of Wind Engineering*, Vol. 40, No. 143, 191-192. (Japanese)

[13] Kishiki S, Ohkawara Y, Yamada S (2008): Experimental evaluation of cycle deformation capacity of u-shaped steel dampers for base isolated structures. *Journal of Structural and Construction Engineering*, Vol. 73, No. 624, 333-340. (Japanese)

